行政院國家科學委員會專題研究計畫 成果報告

新穎材料開發關鍵核心設施計畫--雷射分子束氧化物磊晶平台
研究成果報告(精簡版)

計 畫 類 別 ：個別型
計 畫 編 號 ：NSC 97-3114-M-009-001-
執 行 期 間 ：97 年 08 月 01 日至 98 年 09 月 15 日
執 行 單 位 ：國立交通大學材料科學與工程學系（所）

計 畫 主 持 人：朱英豪
共 同 主 持 人：林諭男、張立

報 告 附 件 ：國外研究心得報告

處 理 方 式 ：本計畫可公開查詢

中 華 民 國 98 年 12 月 11 日

行政院國家科學委員會補助專題研究計畫 ☑ 成 果 報 告
□期中進度報告

新穎材料開發關鍵核心設施計畫
-雷射分子束氧化物磊晶平台

計畫類別： ☑ 個別型計畫 □ 整合型計畫
計畫編號： NSC 97-3114-M-009-001-
執行期間： 97 年 8 月 1 日至 98 年 9 月 15 日

計畫主持人： 朱英豪
共同主持人： 林諭男、張立

成果報告類型(依經費核定清單規定繳交)：☑精簡報告 □完整報告

本成果報告包括以下應繳交之附件：
☑赴國外出差或研習心得報告一份
□赴大陸地區出差或研習心得報告一份
□出席國際學術會議心得報告及發表之論文各一份
□國際合作研究計畫國外研究報告書一份

處理方式：本計畫可公開查詢

執行單位： 交通大學材料工程學系

中 華 民 國 98 年 12 月 10 日

中文摘要

本計劃希望藉由雷射分子束磊晶之建立，可以快速大幅提升我國學界與業界在氧化物磊晶研發之實力。氧化物材料具有多樣之結構特性，可以形成簡單之二元氧化物，亦可形成複雜之多元氧化物，同時包含許多特殊之優良性質，舉凡超導特性、巨磁阻特性、焦電、壓電、介電、半導、導電、磁性、光性等，幾乎包含所有物理性質。氧化物電子目前正蓬勃之發展，為下一個世代之電子元件提供另一種解決方案。計劃要建立之系統雷射分子束磊晶平台，將具有高工作氣壓之 RHEED 來進行臨場薄膜之成長。此一磊晶成長平台建立，可以快速提昇我國於氧化物磊晶成長之基礎能力，可以繼續利用此平台研發新穎與新功能之材料。高品質之材料為固態物理研究之基石，此平台建立後，可以為以量測為主之研究群，提供樣品確保其樣品之品質。另外對於成長氧化物磊晶有興趣之研究群，這樣的平台提供共同研發之機會，可以藉由計畫主持人長期之經驗，快速的建立起新製程，以利其他研究群材料之快速開發。此一平台亦提供業界快速取得多功能與高品質之氧化物磊晶，有助於縮短業界開發新製程與元件之研發時間，同時間由於各種氧化物搭配，亦可由此一平台提供，亦可提供業界元件製程與整合所遇到困難之解決方案。

abstract

Oxide materials are gifted systems, providing a variety of physical properties, including superconducting, ferroelectric, piezoelectric, magnetic, CMR, optical, conducting and et al. The combinations of these properties provide new solutions of next-generation electron devices. The goal of this project is to build up a laser molecule beam epitaxy (MBE) system to fabricate epitaxial oxide heterostructures. Because it has the advantages of high quality epitaxial growth, fast optimization, and good composition and interface control, it has been a core technology on developing oxide heterostructures for many years. Such a platform will greatly promote the ability of studying oxide electronics in academia and industry. Such a system will help us to build up a database for oxide epitaxial growth and to understand the fundamental physics in behind. Such a platform can be used to develop new functional oxide materials and heterostructures. It can also be used to provide high-quality epitaxial oxide films for research groups to do other detail measurements. It can also be used as a platform for industry to develop new oxide devices. It will be an efficient approach to integrate research energy in academia and industry.

關鍵詞： laser MBE, epitaxial, superlattice, termination control

本研究計畫主要建立雷射分子束磊晶成長與檢測平台，用來成長高品質氧化磊晶薄膜，以及快速建立氧化物磊晶薄膜檢測之技術，提供我國學術研究與產業合作之平台。

系統建置

去年已獲補助 1500 萬，建立雷射分子束氧化物磊晶系統。在交大校方與交大材料系上之支援下，提供交通大學工程六館 709 室(30 坪)專屬實驗室，用以建構系統。在實驗設備之支援，由系方建構通風櫃與配電系統，共同主持人援助準分子雷射系統一套，以協助實驗室之建立，同時並提供約 100 萬之配合款，用以協助系統其餘周邊設備之建立。經過對空間之量測，決定系統之建置圖如圖 1 所示。空間之左邊主要提供基板之處理，配有通風櫃，可以進行化學蝕刻以處理基板，經過處理完之基板，可以進入高溫管爐以進行退火，來達到基板表面之控制。空間之右邊為薄膜成長區，目前規畫兩部準分子雷射系統，第一套準分子雷射將配置兩套衛星 PLD 系統，以輔助主系統之運作。因為多數材料在剛開始開發之階段，會遭遇許多製程問題，因此藉由衛星系統之來確定此材料可以進入主系統以進行進一步之製程控制，以避免損壞主系統。兩個系統在規畫上會以不同之材料系統為分界，一套將以氧化物材料為主，另一套則提供非氧化物材料之研發。 在第二套準分子雷射上，主要將建置主系統以及另一套完善之衛星系統。主系統之責任在於準確的控制高品質氧化物磊晶之成長，並配合高壓 RHEED 了解製程參數對於薄膜成長之細部控制。 目前此部分之建置已完成，如圖 2 所示，並以開始進行材料之開發，以提供研究群之使用。

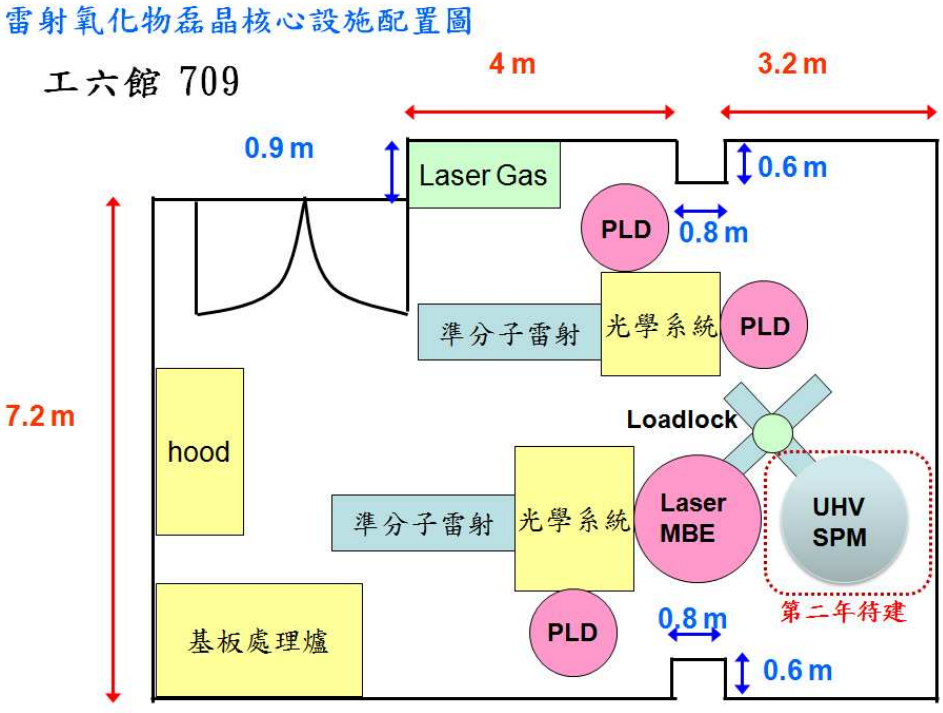

圖 1 專屬實驗室空間規畫圖

圖 2 核心設施之建置實圖

製程開發

基板處理能力之建立為成長高品質薄膜之關鍵步驟，本平台除了提供通風櫃與高溫處理爐外，亦開始建立基板處理之資料庫。 圖 3 為不同晶格常數基板經過化學蝕刻後，在高溫退火完之表面影像圖，可以看見原子台階，證明此平台已有基板處理能力，可以控制基板表面之 termination。

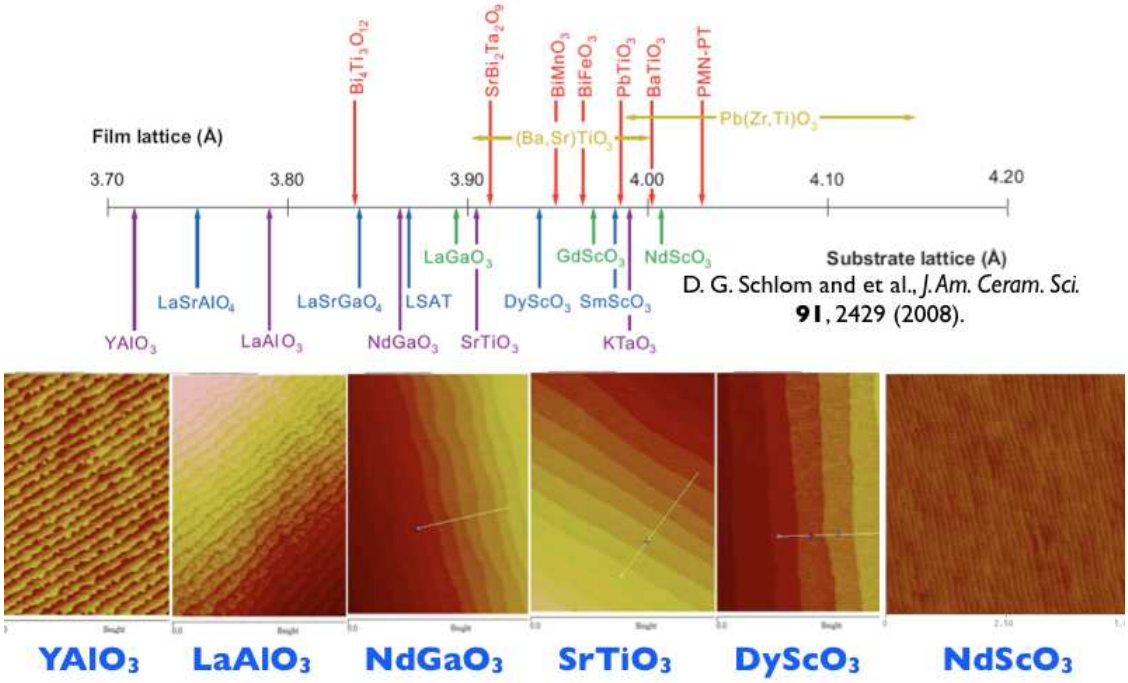

圖 3 不同晶格常數基板經過化學蝕刻後在高溫退火完之表面影像圖

利用已建立之基板處理能力，開始利用已建好之衛星系統，進行氧化物薄膜開發。計畫主持人利用本身之經驗，已陸續完成幾種關鍵材料之製程優化，如：$SrRuO_3$, $LaNiO_3$, YBCO, $La_{0.7}Ca_{0.3}MnO_3$, $La_{0.7}Sr_{0.3}MnO_3$, $La_{05}Sr_{0.5}CoO_3$, $BiFeO_3$, $BaTiO_3$, $PbZr_{0.2}Ti_{0.8}O_3$, $SrTiO_3$, $LaAlO_3$，並已開始提供平台初期參與之研究群高品質之薄膜，以利研究群進行下一步之研究。

在單相材料之開發上，計畫主持人利用 $DyScO_3$ 基板 anisotropy 的特性，在上面成長 $BiFeO_3$ 薄膜，藉由 $SrRuO_3$ 底電極厚度之控制，可以在奈米的尺度下控制薄膜多鐵電域之結構，創造出一維之週期結構，如圖 4 所示，為一創新方法，該結構可以提供一個簡化之材料系統有利進一步了解多鐵域壁之特性，該成果已撰寫論文並已被 Nano Lett. (2009)刊出 [1]。本研究團隊亦利用不同晶格常數之基板開發出 tetragonal 與 orthorhombic 的 BFO，如圖 5 所示，成果領先國際起碼半年以上。

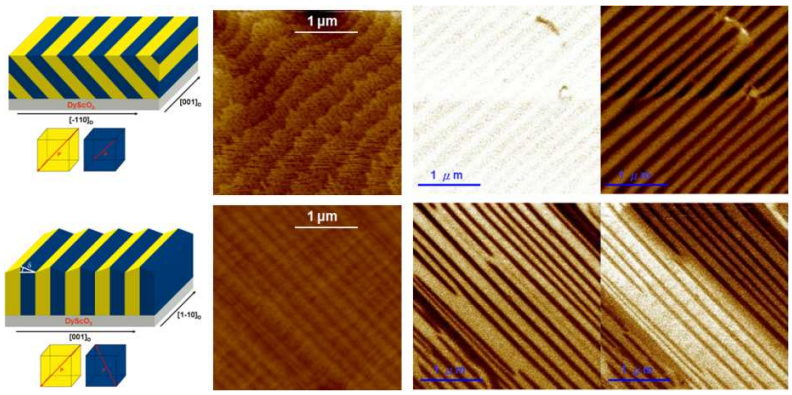

圖 4 BFO/SRO/DSO 之一維奈米週期結構 [1]

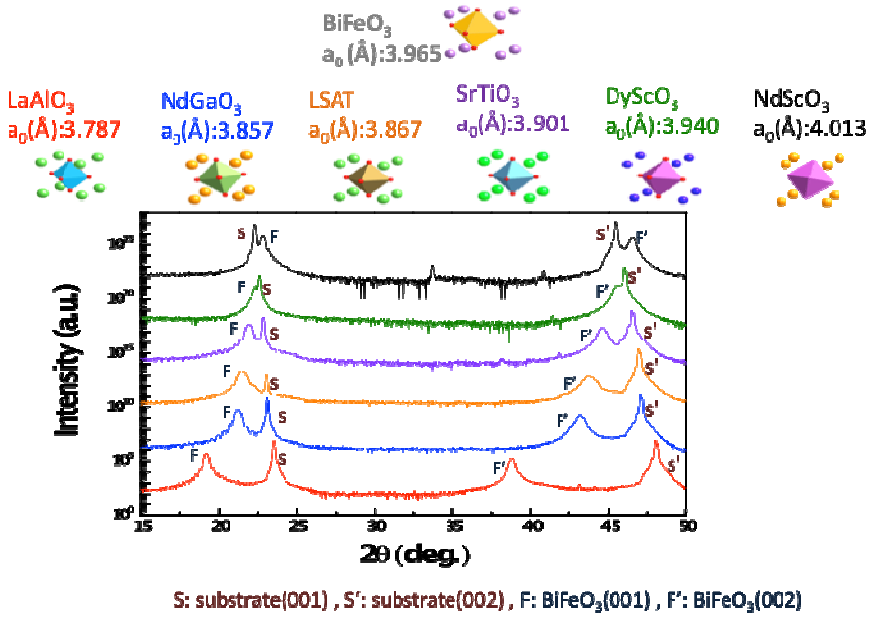

圖 5 利用不同晶格常數基板創造新的 $BiFeO_3$ 相

本研究團隊在薄膜介面之控制亦有所成果，已成功控制 LSMO 與 BFO 兩種材料之介面，藉由 TEM 之觀察發現兩介面之間距有極大之差異，如圖 6 所示會對介面磁性與電性有很大之影響，相關成果與量測持續進行中。 另一種重要的結構為超晶格，研究團隊亦利用主系統開發具有 unit cell 控制能力之 YBCO/LCMO 超晶格結構，如圖 7 所示。這兩種控制的開發展現了本研究團隊具有能力開發出領先國際水準之氧化物磊晶薄膜。

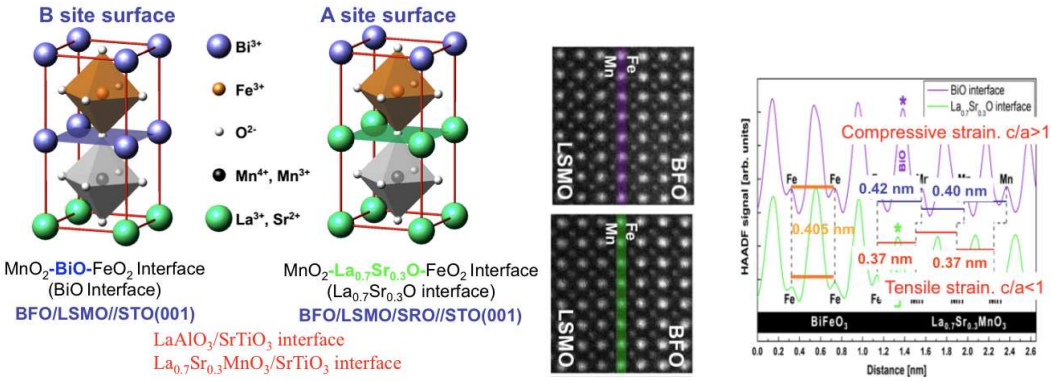

圖 6 控制 LSMO 與 BFO 兩種材料之接面

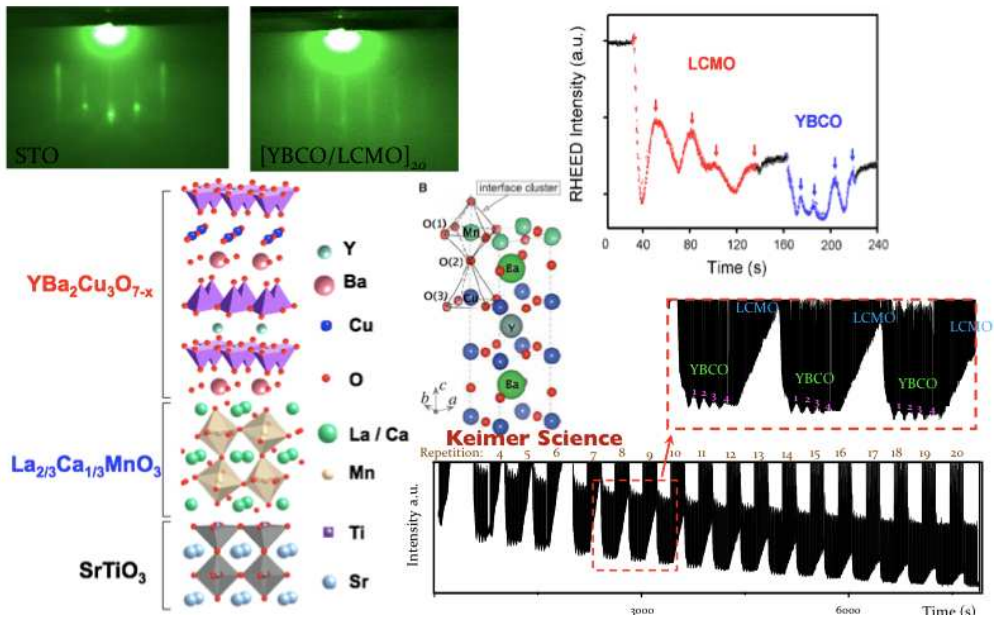

圖 7 磊晶控制 YBCO 與 LCMO 之超晶格結構

國際研究合作

新穎核心設施之計畫概念，在於建立可以提供高品質之材料，以厚植本國在該領域之研發實力。在培養實力之過程，與國外學者之研究合作至為重要。計畫主持人回

國時間不長，但是在國外就與數十個知名之研究團體進行合作，因此在推廣平台之過程，一開始之主要對象亦與國外為主。計畫主持人於寒暑假都前往 UC Berkeley Ramesh's group 進行技術交流。由於計畫主持人具有成長 $BiFeO_3$ 磊晶薄膜之關鍵技術，因此在寒暑假都指導 UC Berkeley 之研究群成長該薄膜，同時也利用台灣現有之系統，提供薄膜與國外研究團體。主要之合作研究成果包含於 2009 年在 Nature Materials 發表 $BiFeO_3$ 多鐵域壁之導電特性[2]，該成果開啟了氧化物材料於奈米元件之新思維，並已被數十個國外新聞網站報導。另一個重要之研究成果為在 $BiFeO_3$ 材料中摻雜 Ca 來創造電洞缺陷，可以使此材料由電場來控制其導電率之大小，提供另一種非揮發性記憶體之選擇，該論文亦已被 Nature Materials 發表[3]。目前能源議題發燒，合作研究方向亦包含開發新式之能源材料，合作成果展示可以利用 $BiFeO_3$ 之鐵電自發極化與電域電場，來產生 PV 效應，提供太陽能轉換之另一種選擇，該論文亦投稿於 Nature Nanotechnology，目前已被接受[4]。

同時間更利用本平台與 UC Berkeley 物理系之 Prof. Orenstein 合作，利用時間解析 THz 光譜，了解 $SrRuO_3$ 之高頻鐵磁共振，該論文已於 PRL 刊登[5]。系統亦提供高品質 $BiFeO_3$ 薄膜給 Prof. Gopalan in Penn State Univ.進行 Raman 光譜學之量測，該論文以刊登於於 Phys. Rev. B[6]。另有一些高品質薄膜提供給美國田納西大學 Prof. Musfeldt 進行光學之量測，該研究成果已經被於 PRB 刊登[7]。另一個合作對象為美國威斯康辛大學之 Prof. Eom，共同研究 $BiFeO_3$ 與控制鐵彈性之轉換，為目前唯一之實驗數據證明可以大面積的控制鐵彈性轉換，該結果論文已撰寫完畢，已投稿於 Nature Mater.[8]。為了要確保平台於氧化物介面之研究方向，可以在最短之時間展現成果，本平台亦與荷蘭 Twente 大學的 Dr. M. Huijben 合作，並進行 LSMO/$BiFeO_3$ 之介面控制，目前有部份成果刊登於 PRB[9]，更重要之結果為利用電場來控制 LSMO 的特性，該結果目前投稿於 Nature Mater.，還在審核階段[10]。計畫主持人與美國 Prof. L. W. Martin 合作多年，目前美國伊利諾大學香檳校區將投入資源建立氧化物磊晶平台，並聘任 Prof. Martin 為計畫領導人，所已計畫主持人持續與 Prof. Martin 合作，雙方之近期成果已投稿 APL[11]，同時接亦受到兩個國際著名期刊之邀稿，將撰寫回顧專文[12,13]。

在掃描探針技術之合作團隊亦沒有因為主持人回台灣而中斷掉，主持人利用衛星系統再度提供高品質之 $BiFeO_3$ 薄膜於雙晶基板上於美國 Oak Ridge 國家實驗室之 Prof. Kalinin，該研究團隊研究鐵電材料於人工晶界上反轉之動力學，目前有一篇論文發表於 APL[14]，另有一篇被 Adv Funct. Mater.接受[15]。同時間該研究團體，並利用平台提供之薄膜進行鐵電 Vortex 結構之研究，該成果已刊登於 Nature Nanotechnology[16]。另一個掃描探針之合作對象為美國康乃狄克大學之 Prof. Huey，主要是由平台提供高品質 PZT 與 $BiFeO_3$ 鐵電薄膜，由該研究群進行超高速壓電力顯微鏡之研究，以了解鐵電薄膜於翻轉動力學，目前 PZT 部分之成果投稿 ACS Nano[17]，其餘之研究成果尚在整理中。在電性量測方面，目前合作之對象有德國 MPI 之 Prof. M. Alexe 與韓國首爾大學 Prof. Kim，與 Prof. Alexe 之研究主要在於

$BiFeO_3$ 薄膜之電性量測，成果已撰寫完畢，部分刊登於 APL[18,19]。與 Prof. Kim 之研究則以 magnetoelectric effect 為主，成果仍在整理中。以上為目前已有具體成果之合作研究團隊，目前仍在合作中的研究團隊包含北京清華大學之 Prof. Yu 與新南斯威爾大學之 Prof. Valanoor。

圖 8 為與國外研究團隊合作之關鍵成果圖，以上之研究成果，證明目前之磊晶平台已具有國際之水準，可以提供國外研究團隊高品質磊晶薄膜，以厚植本國在氧化物磊晶薄膜之研發能力。

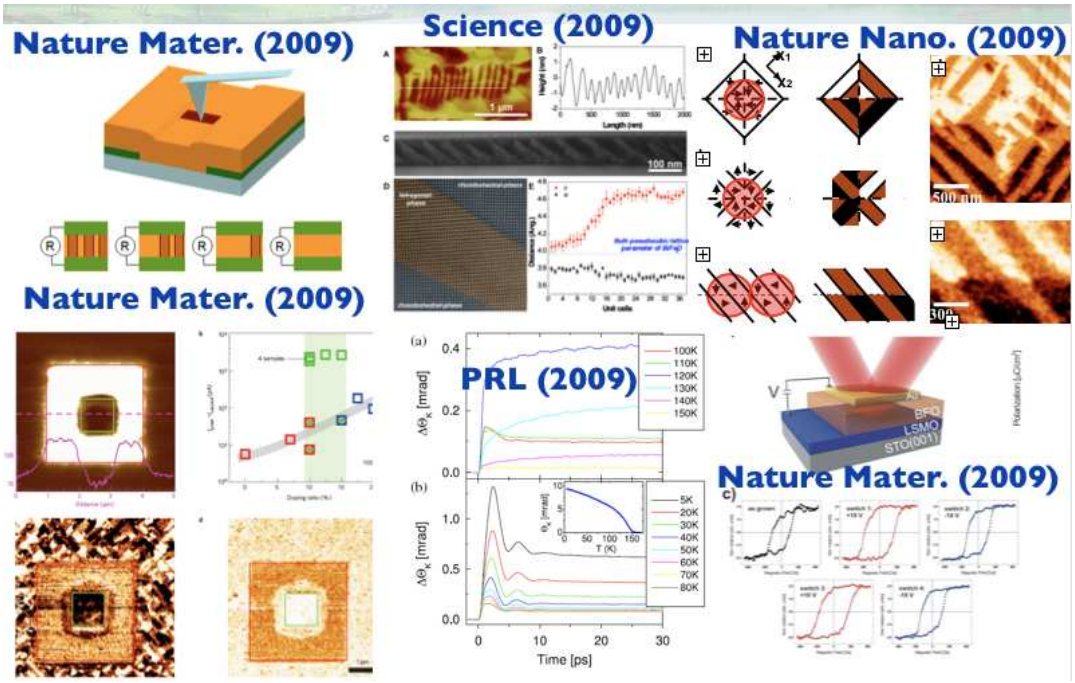

圖 8 與國外研究團隊合作之關鍵成果圖

國內研究合作

與國內之研究起步比較晚，主要是因為計畫主持人剛回國。最早之合作對象為清華大學吳泰伯教授，主要在成長鐵電 PZT 與 $CoFe_2O_4$ 鐵磁材料之多層膜結構，希望可以做出磁電耦合之新材料，目前成果已發表[20]。另外一個合作題目為利用 $BiFeO_3$ 當成電阻式之記憶體之研究，成果尚在整理。另一個主要合作對象為成大物理系陳宜君教授，該研究團體主要專注於掃描探針系統，因此由本計畫之衛星系統，提供高品質之 $BiFeO_3$ 材料，以了解此材料之鐵電轉換機制，目前成果已被 APL 刊出[21]。本計畫另一群重要之合作研究群為交大電物系之固態實驗室(莊振益教授)，該研究群多年深耕於強關聯系統，與本計畫密切結合，目前在多鐵材料之研究，亦有成果，共同發表[22]。

上述幾個研究群皆是已有成果產出，因此與這些研究群之合作關係，會將持續，陸續會有成果產出。另外還有許多國內之研究群之合作屬於起始階段，待雙方磨合期

結束，便開始會有實質之數據產出，以提高平台之利用效率。比如說與同步輻射黃迪靖教授之合作，便想利用軟 X 光來研究各式各樣之複雜氧化物系統。林宏基博士合作了解 strain 對 BFO 材料 crystal field 的影響。台大凝態中心之林昭吟教授，合作 Dy doped $BiFeO_3$ 薄膜之電性與磁性，成大物理系吳忠霖教授合作利用掃描光激發電子顯微鏡了解氧化物材料之介面行為。中山大學物理系邱雅萍教授合作利用 STM 了解氧化物介面之細部行為。清大電子邱博文教授，合作高介電常數閘極材料對碳奈米材料電性之影響。交大材料張立教授則合作開發高功能之 ZnO 薄膜。交大材料吳文偉教授研究 Si 化合物與鐵電材料之整合。交大材料曾院介合作磁性氧化物材料介面之磁性行為。交大電物吳光雄教授與羅志偉教授合作飛秒雷射了解 $BiFeO_3$ 之 THz 響應。交大物理林俊源教授合作新式 $BiFeO_3$ 之磁性。

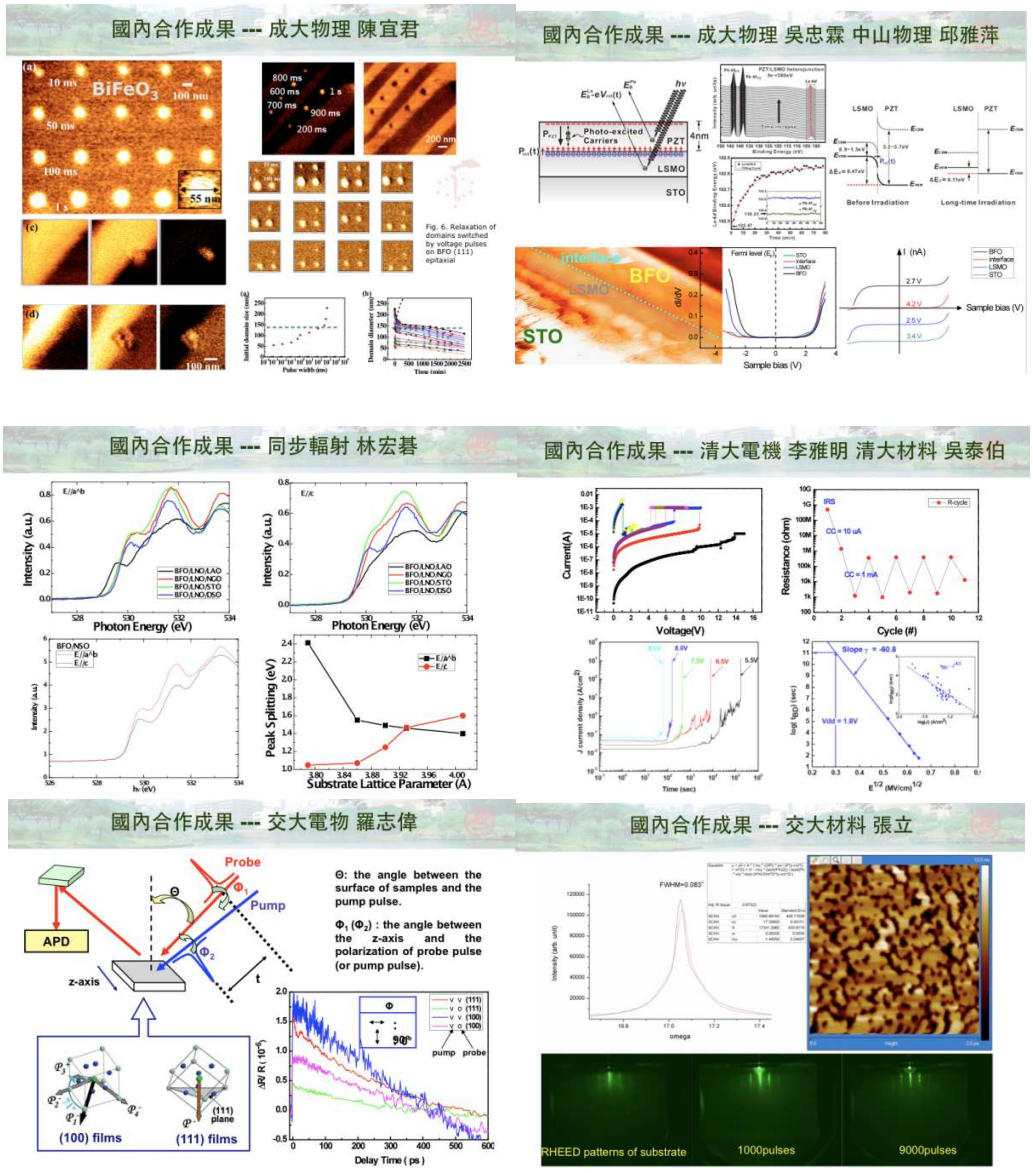

圖 9 與國內研究團隊合作之關鍵成果圖

綜合以上所述，可以得知此平台無論在國外與國內都相當活躍，提供許多研究群高品質之氧化物薄膜，除此外還結合各個領域之研究人才，提供我國在此領域之研究總能量。

參考資料

[1] Y. H. Chu and et al., "Nanoscale Control of Domain Architectures in $BiFeO_3$ Thin Films", *Nano Lett.* **9**, 1726-1730 (2009).

[2] J. Seidel and et al., "Conducting domain walls in oxide multiferroics", *Nature Mater.* **8**, 229 (2009).

[3] C.-H. Yang and et al., "Electric modulation of conduction and ferroelectric states in Ca-doped $BiFeO_3$ films", *Nature Mater.* **8**, 485-493 (2009).

[4] S. Y. Yang and et al., "Domain wall driven anomalous photovoltaic effect on a complex oxide", *Nature Nanotechnol.* accepted (2009).

[5] M. C. Langner and et al., "Observation of ferromagnetic resonance in strontium ruthenate", *Phys. Rev. Lett.* **102**, 177601 (2009).

[6] M. O. Ramirez and et al., "Spin-Charge-Lattice Coupling through Multi-Magnon Excitations in Multiferroic $BiFeO_3$", *Phys. Rev.* B **79**, 224106(2009).

[7] X. S. Xu and et al., "Optical Properties and Magnetochromism in Multiferroic $BiFeO_3$", *Phys. Rev.* B **79**, 134425 (2009).

[8] H. Baek and et al., "Size and time coupled ferroelectric switching path in the oxide multiferroics", *Nature Mater.* revised.

[9] M. Huijben and et al., "Critical Thickness and Orbital Ordering in Ultrathin $La_{0.7}Sr_{0.3}MnO_3$ Films", *Phys. Rev.* B **78**, 094413 (2008).

[10] M. Huijben and et al., "Electrically controlled magnetization in an oxide multiferroic/ferromagnet heterostructure", *Nature Mater.* revised (2009).

[11] L. W. Martin and et al., "Nanoscale Domain Control of $BiFeO_3$ and Exchange Interactions by Thin Film Growth Modes", *Appl. Phys. Lett.*under review (2009).

[12] L. W. Martin and et al., "Multiferroic Thin Films", *J. Mater. Chem.* accepted (2009).

[13] L. W. Martin and et al., "Advances in the Growth and Characterization of Magnetic, Ferroelectric, and Multiferroic Oxide Thin Films", *Mater. Sci. Eng. R.* accepted (2009).

[14] B. J. Rodriguez and et al., "Ferroelectric domain wall pinning at a bicrystal grain boundary in bismuth ferrite", *Appl. Phys. Lett.* **93**, 142901 (2008).

[15] B. J. Rodriguez and et al., "Unraveling Deterministic Mesoscopic Polarization Switching Mechanisms: Spatially Resolved Studies of a Tilt Grain Boundary in Bismuth Ferrite", *Adv. Funct. Mater.* **19**, 2053-2063 (2009).

[16] N. Balke and et al., "Deterministic control of polarization switching in multiferroic materials", *Nature Nanotechnol.* accepted (2009).

[17] R. Nath and et al., "High Speed SPM for Direct Nanoscale Mapping of Nucleation and Growth", ACS Nano submitted (2009).

[18] D. Pantel and et al., “Switching kinetics in epitaxial $BiFeO_3$ thin films”, *Appl. Phys. Lett.* revised (2009).

[19] L. Pintilie and et al., “Orientation dependent potential barriers in case of epitaxial Pt-$BiFeO_3$-$SrRuO_3$ capacitors”, *Appl. Phys. Lett.* **94**, 232902 (2009).

[20] R. Lin and et al., “Interface Effects on the magnetoelectric properties of the (00l)-oriented $Pb(Zr_{0.5}Ti_{0.5})O_3/CoFe_2O_4$ multilayer thin films”, *Scripta Mater.* **59**, 897-900 (2008).

[21] Y. C. Chen and et al., “Domain growth dynamics in single domain like $BiFeO_3$ thin films”, *Appl. Phys. Lett.* **94**, 122908 (2009).

[22] T. H. Lin and et al., “Effects of compressive epitaxial strain on the magnetoelectric properties of the c-axis-oriented orthorhombic $HoMnO_3$ thin films”, *J. Appl. Phys.* **106**, 103923 under review (2009).

Department of Materials Science and Engineering
National Chiao Tung University

國外差旅報告

（一）出差心得

出國申請人朱英豪於二月加入交大材料系，在此之前於 UC Berkeley 物理系擔任博士後研究員長達三年半之時間，積極參與由美國能源部所資助之量子材料科技研發專題，同時間亦參與美國西部奈米科技與元件研發(WINS)，同時具有基礎研究之能力與元件開發之相關經驗。計畫申請人負責之研究中有一極大之部分在於利用雷射分子束磊晶合成高品質氧化物磊晶薄膜之合成，包含各式結構與特性之磊晶薄膜。成長磊晶薄膜涵蓋各式各樣之物理特性，同時也進行各樣磊晶薄膜之間之組合，比如雙層結構之製作或是超晶格材料之合成。所合成之磊晶薄膜除了提供當時計畫所需之要求，同時間又提供來自世界各領域數十個頂尖研究群進行研究，其中包含:電性、磁性、光性、結構等領域，因此在所合成之磊晶薄膜為各個研究群所肯定，同時間訓練與各個領域之人員之溝通，並了解各項分析工具與量測能提供之資訊，同時也知道各種量測可能遭遇之困境與解決之方法，同時亦體會出高研究水準之作品，常常要由各專精領域之人才集體貢獻，才能達到事半功倍之效果，目前無論是自己主導或與他人合作之研究成果於短短三年內已接受發表有三十篇餘論文，同時間在審核或撰寫中之論文亦十篇，也因為如此積極與傑出之成果，亦被數本期刊邀請進行專文之撰寫。因為計畫申請人在傑出表現，尤其於 $BiFeO_3$ 多鐵體之領域論文發表數為世界第二，在多鐵體(Multiferroic)之領域，論文發表數亦排名於世界前五，目前擔任重要國際期刊之審稿人，如: Advanced Materials, APL, JAP, JMR，同時間可以得到第一手之研究資訊。

回到交大任教後，為保持在此研究領域之領先地位，國科會特別資助 1500 萬元，於交大建構氧化物磊晶薄膜系統，申請人為了繼續研究之持續性，在國科會經費支持下於 2008 暑假前往 UC Berkeley 持續相關研究。在加入交大一年多之時間，已發表超過十篇論文，成果多數刊登於重要期刊，如: Nature Mater.，APL，PRL 等。2009 寒假已捨棄與家人團聚之機會在交大校方之經費支持下，前往 UC Berkeley 繼續研究，今年暑假在校方經費支助下，計劃前往美國勞倫斯國家實驗室材料科學部門 Prof. Ramesh 實驗室與 Advanced light source 繼續 2009 寒假所開始之相關研究。該實驗室為目前於此領域之領先實驗室，具有充足的資源，可以快速將目前之實驗構想付諸實現。

（二）短期研究成果

Magnetoelectric coupling in multiferroic materials has attracted much attention because of both the intriguing fundamental science and the significant potential for applications of this phenomenon[1,2]. Among the large number of materials systems currently being explored[3,4],

the model ferroelectric, antiferromagnet $BiFeO_3$ (BFO) has captured a significant amount of research attention, primarily as a consequence of the fact that the two primary order parameters are robust with respect to room temperature (T_C ~ 820°C, T_N ~ 350°C)[5,6]. The original work of Wang *et al.*[7] in 2003 identified several puzzling features of this system. First, the ferroelectric polarization observed in epitaxial thin films was significantly higher (~60 μC/cm^2) than what was published for the bulk at that time. Although provocative at that time, these large values of polarization are now well understood through several theoretical and experimental studies which have confirmed that the ferroelectric polarization of the bulk is indeed quite large and that the originally reported low values of ferroelectric polarization were likely the consequence of leakage in the material that prevented the application of a large enough field to saturate the polarization state[8].

The second provocative observation in that paper was the existence of a relatively large magnetic moment in thin films, which was considerably larger than the expected value from the canted antiferromagnetism (~8 emu/cm^3)[9]. This led to a significant amount of discussion and follow up work within the community in attempts to better understand the origins of this enhanced moment. Eerenstein *et al.*[3] proposed that the excess magnetism was associated with magnetic second phases (such as γ-Fe_2O_3); this was supported by the studies of Béa *et al.*[10] who showed that BFO films, when grown under reducing conditions (for example under oxygen pressures lower than 1x10^{-3} Torr) showed enhanced magnetism as a consequence of the formation of magnetic second phases. It is however important to note that low oxygen pressure during growth is not the cause for the enhanced moment in the 2003 report[7] where films were grown in oxygen pressures between 100-200 mTorr and cooled in 760 Torr – rendering formation of such secondary magnetic phases thermodynamically unlikely. More recently, the work of Martin *et al.*[11] suggested the role of thin film processing (for example the growth rate) as a possible parameter that influences the state of magnetism in the film through control of the ferroelectric domain structure. Finally, the recent observation of enhanced electrical conduction at specific types of ferroelectric domain walls (namely 109° and 180° walls)[12] provides another important context to explore in detail the connection between domain wall structure, electronic structure, and magnetism in these complex materials.

In any system with two order parameters, e.g. polarization and magnetization, the coupling between them means that the suppression and/or gradient of one order parameter at its domain wall must necessarily affect the other. In other words, the suppression of polarization at the ferroelectric wall must necessarily produce a change in magnetization. Thus, even if the magnetization is zero within the domains, it will be non-zero at the domain walls. This general idea can be understood within the framework of a classical Landau theory. Starting from the simplest thermodynamic potential incorporating two order parameters expanded up to quartic order (the minimum required for a second order phase transition, though we note here that the ferroelectric transition in BFO is almost certainly first order) and biquadratic coupling between the two order parameters (biquadratic coupling is always allowed by symmetry, and therefore always present in any system with two order parameters).

Because biquadratic free energy terms such as P^2M^2 are scalars in any symmetry group, this potential can be written thusly:

$$G_{MP} = G_0 + \frac{\kappa}{2}(\nabla P)^2 + \frac{\lambda}{2}(\nabla M)^2 + L_{MP}(P,M) = G_0 + \frac{\kappa}{2}(\nabla P)^2 + \frac{\lambda}{2}(\nabla M)^2 + \frac{\alpha}{2}P^2 + \frac{\beta}{4}P^4 + \frac{a}{2}M^2 + \frac{b}{4}M^4 + \frac{\gamma}{2}P^2M^2$$ When one goes from $+P$ to $-P$, it is energetically more favorable for the domain wall energy trajectory not to go through the centre of the landscape (P=0, M=0), but to take a diversion through the saddle points at $M_0 \neq 0$, thus giving rise to a finite magnetization (Fig. 1). The absolute values of the magnetic moment at the domain wall will depend on the values of the Landau coefficients. The work of Goltsev *et al.* also identified the role of piezomagnetic coupling between a ferroelectric and antiferromagnetic domain wall, again leading to local moments centered at the domain wall. Equally important and relevant is the conclusion that the antiferromagnetic domain wall width can be significantly larger than the ferroelectric domain wall width.

With this as the background, we set out to explore the role of ferroelectric domain formation on the magnetic properties of BFO thin films. The structure of domain walls in ferroelectric perovskites and related materials has been the focus of several prior studies[13,14,15]. In tetragonal ferroelectrics such as $PbTiO_3$, two types of domain walls exist, namely 90° and 180° domain walls. In contrast, rhombohedral ferroelectrics (such as BFO) exhibit three types of domain walls, namely those characterized by a 71° rotation of the polarization vector (71° walls), a 109° rotation (109° walls), and the classic 180° rotation. The first two are both ferroelectric as well as ferroelastic; 71° walls form on 101-type planes (which are symmetry planes for this structure) while 109° walls form on 100-type planes (which are not symmetry planes for the rhombohedral structure)[16,17]. The orientation of the polarization vector changes abruptly at the domain walls, which has already been confirmed by transmission electron microscopy.[18] This can result in the symmetry inside the domain walls being different from that in the domains and, in turn, the properties at the walls can also be different. Indeed, prior theoretical work has predicted that the domain walls in multiferroics can be ferromagnetic even if the domains themselves are antiferromagnetic or paramagnetic[19,20,21]. Conversely, spin rotation across the walls of magnetic insulators can induce a polarization in the walls of otherwise non-polar materials[2,22]. The interaction between ferroelectric and antiferromagnetic domain walls has been studied in model multiferroics such as $YMnO_3$ and $BiFeO_3$. In both cases it has been shown that the antiferromagnetic domain walls are significantly wider (by ~1-2 orders of magnitude) compared to the ferroelectric walls.

In order to study the properties of domain walls, it is imperative that we are able to create controlled arrays of 71° and 109° domain walls in thin film form. We have been able to achieve this using an epitaxial growth process that enabled control over the electrostatic and elastic boundary conditions. First, in order to minimize the lattice mismatch strain, we chose a single crystal, $(110)_{orthorhombic}$ $DyScO_3$ (DSO) substrate (lattice mismatch with BFO is only ~0.2%); then, to manipulate the electrostatic boundary conditions, we used an epitaxial $SrRuO_3$

(SRO) layer of varying thickness as a bottom electrode, all layers being grown by pulsed laser deposition.[23] The ferroelectric domain structures of these two kinds of domain wall samples were characterized using atomic force microscopy (AFM) (Digital Instruments, Nanoscope-IV Multimode AFM) with the cantilever scanning along $<110>_{pc}$(where pc represents the pseudo-cubic structure). Piezoresponse force microscopy (PFM) is used to analyze the ferroelectric domain structure of these films – detailed analysis allow us to determine the individual polarization direction of each domain. We note that detailed structural characterization studies on all of our samples using x-ray diffraction, AFM, and low resolution transmission electron microscopy show no evidence for the formation of second phase material in any samples.

Films grown on a thick SRO electrode (i.e., > 10 nm) show a ferroelectric domain structure that is essentially comprised of periodic arrays of 71° domains (Fig. 2a). A detailed description of the nature of polarization in each domain is shown in Fig. 2b. The out-of-plane (OOP) PFM image (Fig. 2c) of such a 71° domain wall sample shows a uniform contrast, indicating a single OOP polarization component that is downward directed (toward the SRO electrode); the in-plane (IP) PFM image (Fig. 2d) shows a stripe pattern with bright and neutral contrast, which shows that the IP component of the polarization in the bright domains is pointing in $[-110]_{pc}$ direction while the domains with neutral contrast point in the $[-1-10]_{pc}$ direction. As a consequence of such a domain structure, the net IP component of the polarization of the whole sample points along $[-100]_{pc}$. When the SRO bottom electrode thickness is reduced to below ~10 nm (for this study we have used 5 nm), however, the domain structure changes to become predominantly comprised of 109° domains (Fig. 2e). Again, a detailed description of the polarization directions in each domain in this structure is given in Fig. 2f. In contrast to the 71° domain wall structures, both the OOP and IP PFM images of the 109° domain wall samples show stripe-like contrast (Fig. 2g and h, respectively). The OOP PFM image shows two contrasts, dark and bright (Fig. 2g), corresponding to the OOP component of the polarization pointing down and up, while the IP PFM image (Fig. 2h) has three contrast levels, dark, neutral and bright. Dark and bright contrast correspond to the IP component of the polarization pointing in $[1-10]_{pc}$, and $[-110]_{pc}$ directions in different ferroelectric domains as shown in Fig. 2e, while neutral contrast correspond to the IP component of the polarization pointing either in $[-1-10]_{pc}$ or $[110]_{pc}$ directions. It is noteworthy that bright and neutral (or dark and neutral) domains are usually grouped together to form a bright (dark) "domain bands". Within such bright and dark domain bands, the net polarization is directed in opposite IP directions. To confirm the true nature of these domain walls, we have completed high resolution transmission electron microscopy (HRTEM). Atomic resolution images of both types of walls were obtained using the aberration-corrected microscope (TEAM 0.5) at the National Center for Electron Microscopy. These images, (Supplementary Fig. S2) show that the 109° domain walls are ~2 nm (5 unit cells) wide and, indeed, form on the 100-type planes while the 71° walls, which are ~2 nm wide, form on the 101-type planes of the rhombohedral structure (described with the pseudo-cubic notation).

Heterostructures of Pt (2nm)/$Co_{0.9}Fe_{0.1}$ (CoFe) or Co (2.5nm) were grown at room temperature on BFO/DSO samples with both 71° and 109° domain wall arrays in an ion beam sputtering system with a base pressure of ~$5x10^{-10}$ Torr. In traditional exchange bias systems, the effect is only observed upon cooling the system through the Néel temperature of the antiferromagnet in the presence of an external applied field. In our system, heating to above T_N=370°C resulted in interdiffusion of the layers and oxidation of the CoFe films. We have therefore circumvented this issue by growing the CoFe films in an applied field of 200 Oe, so as to induce a uniaxial anisotropy. The magnetic response of the ferromagnetic layer was measured by means of the surface magneto-optical Kerr effect (SMOKE) technique. An incident beam was focused onto the sample surface by an optical lens and polarized in the plane of incidence (*p* polarization). The angle of the incidence of the light was 45° from the sample normal. Upon reflection from the sample surface, the light passed through an analyzing polarizer set at 1° from extinction. The Kerr intensity is then detected by a photodiode and recorded as a function of the in-plane applied magnetic field *H* to generate the hysteresis loop.

Heterostructures created on BFO films with a 71° domain structure showed no exchange bias (Fig. 3a) with applied magnetic field either parallel or perpendicular to the domain walls. On the other hand, samples created from BFO films with 109° domain walls exhibited strong exchange bias behavior. In order to fully understand the details of the origins of the exchange bias, we have applied the growth field of CoFe both parallel and perpendicular to the 109° domain wall surface and negative exchange bias was observed in both cases (Fig. 3b and 3c, respectively). For samples with the growth field applied along the domain wall direction (Fig. 3b), a strong, negative shift of the magnetic hysteresis loop (typical exchange bias field ~40 Oe) is observed while applying the measurement field antiparallel to the growth field of the CoFe (red curve, Fig. 3b). When the measurement field is applied perpendicular to the growth field of CoFe layer, the magnetic response exhibited a hard axis behavior, which shows negligible shift of the hysteresis loop (blue curve, Fig. 3b). We also note that we observe the opposite shift of the hysteresis loop when measured parallel to the growth field of CoFe, thus confirming the behavior to be a classical exchange bias interaction. Similar effects were observed in samples where the growth field was applied perpendicular to the domain wall direction (Fig. 3c). Additionally, the magnitude of the exchange bias is observed to scale directly with the density of 109° domain walls in the sample (Fig. 3d). It is also interesting to note that the domain wall density dependence is much stronger for films grown on [100] $SrTiO_3$ substrates[11]; this clearly suggests a strong contribution from the domain wall topology (i.e., the 109° domain walls in films grown on STO substrates have a tortuous topology while the walls in films grown on DSO substrates are crystallographic in nature, Fig. S2), and possibly from a difference in the strain state in the BFO layer on these two substrates.[24]

The correlation between exchange bias and domain wall tortuosity is also geometrically consistent. Recent studies of irregular domain walls in BFO films[25] show that these can be characterized by a fractal Hausdorff dimension bigger than two, meaning that the domain walls

occupy a much larger volume fraction than might be expected from flat or smooth walls. The larger volume ratio occupied by the fractal walls would account for their bigger contribution to the average macroscopic magnetization. Moreover, irregular domain walls are necessarily non-equilibrium uncompensated structures where a larger fraction of uncompensated spins may be expected.

From these exchange coupling studies two major points can be made: 1) the ferromagnetic CoFe layer experiences a directional exchange bias *only* when deposited on a BFO layer that has a large density of 109° domain walls, suggesting the existence of pinned, uncompensated spins in the BFO layer at such domain walls as the direct origin of this exchange bias; 2) that the direction of the exchange bias shift if dictated by the application of an external magnetic field (the growth field of 200 Oe).

These exchange bias studies suggest some intriguing differences in the magnetic behavior between the two types of domain structures. To better understand this, it is important to understand the nature of coupling in these exchange coupled systems. In the classical picture of exchange bias, a ferromagnet (FM) is in contact with a fully uncompensated antiferromagnet (AFM) surface that presents pinned, uncompensated spins that interact with the spins in the FM, leading to an anisotropic exchange coupling. It has been proposed that these pinned, uncompensated spins can arise from a multitude of sources, such as the surface termination of crystallographic planes in the AFM, roughness of the interface between the FM and AFM, structural defects, and grain boundaries or domain structures in the AFM.[26,27,28] Thus, we first discuss this various possibilities before presenting photoemission experiments that will help unravel the origin of these pinned spins in the present BFO-based system.

A perfectly ordered, atomically-abrupt (001) surface for a single domain of the G-type antiferromagnet such as BFO is a fully compensated surface (i.e., possessing equal number of antiparallel spins); thus such a surface termination is not expected to lead to an exchange bias effect. Therefore, to first order, we can eliminate the domain surface as the source of uncompensated spins. It is also possible that differences in surface morphology between the 109° domain wall samples (which have a twinned surface with alternating tilts arising from the structural distortion of the rhombohedral structure), and the 71° domain wall samples, which have flat surfaces with roughness on the order of atomic steps, could play a role in the different exchange bias properties. Fig. 4a illustrates the surface topography of the film containing 109° domain walls schematically. From x-ray diffraction and HRTEM studies, the surface planes on the two sides of a 109° domain wall are tilted by an angle of *only* 0.3°[23]. However, the domain surface itself is still a fully compensated surface and as such is not expected to give rise to uncompensated spins or exchange bias. We therefore focus on the magnetic structure of the domain walls, (i.e., at the ridges or troughs of the corrugated surfaces). Fig. 4b illustrates the four possible polarization variants that can come together at this interface to create the 109° domain wall. Also shown in this figure are the antiferromagnetic vectors, *L*, and the corresponding canted moment, *M*. In epitaxial films of BFO, previous work[29] has

demonstrated that the easy plane antiferromagnetic structure of BFO[9] is broken by epitaxial strain imposed by the substrate; in the case of both STO and DSO substrates, this leads to the formation of a $<112>_{pc}$ easy axis for *L*; the corresponding *M* lies along $<1\text{-}10>_{pc}$ or $<\text{-}110>_{pc}$. With a canting angle of ±1°[9], the canted moment *M* gives us two possible configurations for the *M* in adjacent domains across a 109° domain wall (Fig. 4c and d, respectively).

As an illustrative example, if we fix the ferroelectric polarization *P* along $[\text{-}111]_{pc}$, then *L* is along $[1\text{-}12]_{pc}$, and *M* points along $[110]_{pc}$, as shown by the arrows in the yellow block (Fig. 4c and d). On the other side of the wall (shown as the green block), *P* is along $[\text{-}1\text{-}1\text{-}1]_{pc}$, *L* along $[\text{-}1\text{-}12]_{pc}$, and *M* can point along either $[1\text{-}10]_{pc}$ (Fig. 4c) or $[\text{-}110]_{pc}$ (Fig. 4d). The transition area (i.e, the 109° domain wall) can be thought of as a Néel wall that rotates the *M* vector with an enhanced magnitude, which gives us a net magnetic moment, M_{net}, within the wall lying either perpendicular (Fig. 4c) or parallel to the domain wall (Fig. 4d). Upon application of an applied magnetic field during the growth of the CoFe layer, we effectively break any degeneracy between the two configurations and select one over the other. Thus, application of a growth field perpendicular to the domain walls gives rise to the configuration in Fig. 4c and exchange bias in that direction while application of the growth field parallel to the domain wall gives rise to the configuration in Fig. 4d and exchange bias in that direction as is indeed observed experimentally (Fig. 3). With this as the fundamental framework, we proceeded to probe the state of magnetism in the samples, with a specific focus on the samples with 109° domain walls.

Magnetic measurements of nanoscale features is a challenging undertaking. Macroscopic measurements of the magnetic moment of an entire film (for example using SQUID magnetometry) is difficult because of the large relative volume and paramagnetic background of the DSO substrates. Therefore, in order to obtain insight into the local magnetic properties, we have turned to element-specific x-ray spectromicroscopic techniques. Specifically, we have obtained x-ray absorption spectra (XAS) at the Fe *L*-edge using circularly polarized soft x-rays, at a grazing incidence ($\theta = 16°$), while rotating the sample about the surface normal (here we show data for three angles, $\phi = 0°, 90°, 180°$) of the 109° domain wall sample (Fig. 5a). Additionally, spatially resolved photoemission electron microscopy (PEEM) images were obtained using both left- and right-circularly polarized x-rays. In order to enhance the difference in the image contrast between left- and right-ciruclarly polarized (LCP and RCP) light, we have taken the ratio of the two images and report those here[30]. The image contrast is an effective map of the local magnetization vector; regions that have their magnetic moment aligned parallel to the light wave vector show bright contrast, while those that are antiparallel appear in dark contrast. Further details of the experimental procedures are given in the Methods section.

Angle-dependent XMCD-PEEM images were taken with the incident x-rays at various angles to the 109° domain walls; parallel to the domain walls ($\phi = 0°$, Fig. 5b), 180° from this configuration ($\phi = 180°$, Fig. 5c), and perpendicular to the domain walls ($\phi = 90°$, Fig. 5d). For reference, Fig.5e is the corresponding in-plane PFM image of the same region,

in which the image contrast can be understood based on the analysis presented in Fig. 2. We begin by discussing the PEEM images taken at 180° rotations from one another (Fig. 5b, c). The first, and possibly most striking, feature is the observation of dark and bright "bands" of contrast in the image in Fig. 5a; the same features reverse their contrast upon rotation of the sample by 180° (Fig. 5b), clearly identifying the origin of the contrast to be magnetic in nature (pyromagnetic and/or ferromagnetic).

We note that due to the resolution limits of the PEEM technique (PEEM at the SLS has a spatial resolution of ~70nm under ideal conditions), we do not resolve the magnetic information from each of the domains individually,. What is noteworthy, however, is the fact that bands of 109° domains (consisting of an aggregate of individual 109° domains, all with the *same* net in-plane polarization component, Fig. 2c) also have the same net magnetization direction. This is evident by comparing the image contrast in Fig. 5b and the corresponding PFM image in Fig. 5e. Finally, upon rotation by 90° (Fig. 5d), i.e., incident x-rays perpendicular to the direction of 109° domain walls, the PEEM image also shows contrast between these 109° domain bands. This suggests that there is a component of the magnetic moment at 109° domain walls that is perpendicular to the domain wall direction; this is qualitatively consistent with the model in Fig. 3 and the exchange bias measurements.

To further validate the conclusions from the PEEM images in Fig. 4, we carried out detailed spectroscopic measurements a different points throughout the studied area. First, we switched rectangular portions of the film using the PFM; one such region is outlined with a blue box in Fig.5b and is also evident in Fig. 5e. Upon electrical switching, the 109° domains disappear and are replaced with either a single domain state or with 71° domain walls. Thus, it can be hypothesized that electrical switching of the 109° domains into arrays of 71° domains should lead to a change in the overall magnetic state of that region. Using circularly polarized light, x-ray absorption spectra (XAS) were obtained from within the switched area as well as from outside; a typical spectrum is shown in Fig. 6. The normalized difference spectra (i.e., the asymmetry between two XAS spectra) between the switched and unswitched regions gives us a qualitative measure of the difference in ferromagnetic moment between these two areas. The difference spectrum (Fig. 6) for one set of locations (plot in black in Fig. 6) shows an asymmetry of ~1% at the Fe-edge (the inset shows a part of the difference spectrum at the edge). When the polarization of the incident x-ray is changed from RCP to LCP, the shape of XMCD curve obtained from these red and blue boxed areas is reversed (inset). In contrast, when we obtained the difference spectrum from within the switched area, (orange and pink boxes) the asymmetry of the spectra is below the noise level, indicating very little remanent moment. We note that samples with an as-grown 71° domain structure (Fig. 2a, b) consistently show the same behavior as the switched location, namely no measurable asymmetry in the spectra.

In summary, we have systematically studied the magnetic nature of 109° and 71° ferroelectric domain walls in BFO multiferroic thin films and observed enhanced magnetic moments along 109° domain walls, while 71° domain walls show no such enhanced magnetic

moment. Such enhancement is attributed to the symmetry change at 109° domain walls leading to an increase of canted angle between neighboring Fe spins[31]. The nature of the antiferromagnetic domain wall (i.e., its width, the magnitude of the local magnetic moment within the wall) as well as the strength of the coupling between the ferroelectric and antiferromagnetic walls in BFO are issues that still need resolution, both from a theoretical and experimental perspective. BFO films grown on STO substrates (which have a larger in-plane compressive strain of ~2%) compared to DSO (0.3%) show a much more complicated 109° domain structure as well as a higher degree of strain induced tetragonality for the same film thickness[24]. It is quite likely that the enhanced strain as well as the more complex domain wall topology is likely to further enhance the possibility of obtaining larger moments at the domain walls. However this very complexity is also likely to give a large variability in the observed magnetic moments as has been observed in the case of films grown on STO substrates (~30 emu/cc to ~60 emu/cc). This is quite consistent with the experimental observation of a significantly higher exchange bias for the case of films grown on STO substrates compared to those on DSO, Fig. 3d. These results also conclusively show that if the primary domain structure is comprised of 71° domain walls, enhanced moments should not be expected; indeed such samples consistently exhibit a saturation moment in the 6-8 emu/cc (which is the magnitude of the canted moment). Finally, we believe that such broken symmetries at domain walls and structural interfaces are good candidates to look for the emergence of behavior that is deviated from bulk[32].

References

1. Cheong, S.-W. & Mostovoy, M. Multiferroics: a magnetic twist for ferroelectricity, *Nature. Mater.* **6**, 13 (2007).
2. Ramesh, R. & Spaldin, N. A. Multiferroics: progress and prospects in thin films, *Nature Mater.* **6**, 21 (2007).
3. Eerenstein, W., Mathur, N. D., Scott, J. F. Multiferroic and magnetoelectric materials, *Nature* **442**, 759 (2006).
4. Khomskii, D. Classifying multiferroics: Mechanisms and effects, *Physics* **2**, 20 (2009)
5. Roginska, Y. E., Tomashpolsky, Y. Y., Venevtse, Y. N., Petrov, V. M. & Zhdanov, G. S. Nature of dielectric and magnetic properties of $BiFeO_3$. *Sov. Phys. JETP* **23**, 47 (1966).
6. Kiselev, S. V., Ozerov, R. P. & Zhdanov, G. S. Detection of magnetic order in derroelectric $BiFeO_3$ by neutron diffraction. *Sov. Phys. Dokl.* **7**, 742 (1963).
7. Wang, J. *et al.* Epitaxial $BiFeO_3$ Multiferroic Thin Film Heterostructures, *Science* **299**, 1719 (2003).
8. Lebeugle, D. *et al.* Very large spontaneous electric polarization in $BiFeO_3$ single crystals at room temperature and its evolution under cycling fields, *Appl. Phys. Lett.* **91,** 022907 (2007).
9. Ederer, C. & Spaldin, N. A., Weak ferromagnetism and magnetoelectric coupling in bismuth ferrite, *Phys. Rev. B* **71**, 060401 (R) (2005).
10. Béa, H. *et al.* Investigation on the origin of the magnetic moment of $BiFeO_3$ thin films by advanced x-ray characterizations, *Phys. Rev. B* **74**, 020101(R) (2006).
11. Martin, L. W. *et al.* Nanoscale control of exchange bias with $BiFeO_3$ thin films, *Nano Lett.* **7**, 2050 (2008).
12. Seidel, J. *et al.* Conduction at domain walls in oxide multiferroics, *Nature Mater.* **8**, 229 (2009).
13. Wu, X. & Vanderbilt, D. Theory of hypothetical ferroelectric superlattices incorporating head-to-head and tail-to-tail 180° domain walls, *Phys. Rev. B* **73**, 020103(R) (2006).
14. Thomas, L. *et al.* Resonant amplification of magnetic domain-wall motion by a train of current pulses, *Science* **315**, 1553 (2007).
15. Floquet, N. & Valot, C. Ferroelectric domain walls in $BaTiO_3$: Structural wall model interpreting fingerprints in XRPD diagrams, *Ferroelectrics* **234**, 107 (1999).
16. Streiffer, S. K. *et al.* Domain patterns in epitaxial rhombohedral ferroelectric films. I. Geometry and experiments, *J. Appl. Phys.* **83** 2742 (1998).
17. Romanov, A. E. *et al.* Domain patterns in epitaxial rhombohedral ferroelectric films. II. Interfacial defects and energetics, *J. Appl. Phys.* **83** 2754 (1998).
18. Jia, C.-L. *et al.* Atomic-scale study of electric dipoles near charged and uncharged domain walls in ferroelectric films , *Nature Mater.* **7**, 57 (2008).
19. Přívratská, J. & Janovec, V. Pyromagnetic domain walls connecting antiferromagnetic non-ferroelastic magnetoelectric domains, *Ferroelectrics* **204**, 321 (1997).

20. Přívratská, J. & Janovec, V. spontaneous polarization and/or magnetization in non-ferroelastic domain walls: Symmetry predictions, *Ferroelectrics*, **222**, 23 (1999).
21. Goltsev, A. V., Pisarev, R. V., Lottermoser, Th. And Fiebig, M. Structure and interaction of antiferromagnetic domain walls in Hexagonal $YMnO_3$. *Phys. Rev. Lett.* **90**, 177204 (2003).
22. Mostovoy, M. Ferroelectricity in spiral magnets, *Phys. Rev. Lett.* **96**, 067601 (2006).
23. Chu, Y.-H. *et al.* Nanoscale control of domain architectures in $BiFeO_3$ thin films, *Nano Lett.* **9**, 1726 (2009).
24. Chu, Y.-H. *et al.* Ferroelectric size effects in multiferroic $BiFeO_3$ thin films, *Appl. Phys. Lett.* **90**, 252906 (2007).
25. Catalan, G. *et al.* Fractal dimension and size scaling of domains in thin films of multiferroic $BiFeO_3$, *Phys. Rev. Lett.* **100**, 027602 (2008).
26. Malozemoff, A. P., Random-field model of exchange anisotropy at rough ferromagnetic-antiferromagnetic interfaces, *Phys. Rev. B* **35**, 3679 (1987).
27. Takano, K., Kodama, R. H., Berkowitz, A. E., Cao, W. and Thomas, G., Interfacial uncompensated antiferromagnetic spins : Role in unidirectional anisotropy in polycrystalline $Ni_{81}Fe_{19}$/CoO bilayers, *Phys. Rev. Lett.* **79**, 1130 (1997).
28. Scholl, A., Nolting, F., Seo, J. W., Ohldag, H., and Stöhr, J., Domain-size-dependent exchange bias in Co/$LaFeO_3$, *Appl. Phys. Lett.* **85**, 4085 (2004).
29. Holcomb, M. B. *et al.* Probing the evolution of antiferromagnetism in multiferroics, *Phys. Rev. B*, revised (2009).
30. Nolting, F. *et al.* Direct observation of the alignment of ferromagnetic spins by antiferromagnetic spins, *Nature* **405**, 767 (2000).
31. Lubk, A., Gemming, S. and Spaldin, N. A., First-principles study of ferroelectric domain walls in multiferroic bismuth ferrite, *Phys. Rev. B* in press (2009).
32. Noheda, B., MRS Fall talk (2008).

Figure Captions

Figure 1 Evolution of polarization and magnetization at domain walls in $BiFeO_3$. Calculations reveal that (a) the polarization is zero at the center of a 109° domain wall, but has a finite value in the domains themselves, while (b) the magnetization is finite in the center of domain walls, but zero in the domains (Figures courtesy of Ref. X). (c) *M(x)* and *P(x)* are constrained on an ellipse; (d) The free energy shows two minima at $P=\pm P_0$. The system will move from one of those minima to the other not through the centre of the diagram but through its saddle points. This will give an increase of *M* in the center of the ferroelectric domain walls. X-Axes in (a), (b) and (d) are in arbitrary units.

Figure 2 Understanding domain structures in rhombohedral ferroelectrics. (a) Schematic of 71° domain pattern. Domain colors are following from IP-PFM image as shown in (d). Green arrow shows the net ferroelectric polarization. (b) Schematic of detailed 71° domain structure with blue arrows showing the ferroelectric polarization components in $[001]_{pc}$ and $[010]_{pc}$ planes. (c)(d) OP and IP-PFM images of 71° domain pattern. (e) Schematic of 109° domain pattern with different domain clusters. Domain colors are following the contrast of IP-PFM image as shown in (h). Green arrow shows the net ferroelectric polarization within each domain cluster. (f) Schematic of detailed 109° domain structure within one domain cluster. Blue arrows show the ferroelectric polarization components in $[001]_{pc}$ and $[010]_{pc}$ planes. (g)(h) OP and IP-PFM images of 109° domain pattern.

Figure 3 Exchange bias on 109° and 71° domain wall samples. (a) Hysteresis loop of CoFe on 71° domain wall sample. Red (blue) curve corresponds to the applied magnetic field antiparallel (perpendicular) to the grown magnetic field of CoFe. (b) Hysteresis loop of CoFe on 109° domain wall sample with growth field along the direction of 109° domain walls. (c) Hysteresis loop of CoFe on 109° domain wall sample with growth field perpendicular to the direction of 109° domain walls. (d) Dependence of exchange bias field on density of 109° domain walls for CoFe/BFO heterostructures grown on 109° domain wall samples.

Figure 4 Magnetism model of 109° domain walls in $BiFeO_3$. (a) Domain structure separated by 109° domain walls shown in crystal unit cells. Blocks with different colors are corresponding to the unit cells with different ferroelectric polarization and Fe spins as shown in (b). (b) Yellow arrows show the ferroelectric polarization P; purple arrows show the Fe spins in every unit cell. (c) Configuration of 109° domain wall with a net magnetic moment pointing out of the wall plane. Red arrows in the unit cells show the direction of the canted moment. (d) Configuration of 109° domain wall with a net magnetic moment laying in the wall plane.

Figure 5 Photoemission electron microscopy studies of $BiFeO_3$. (a) Schematic illustrating the experimental geometries used to take PEEM images of 109° domain walls with circular polarized x-ray. (b) PEEM image obtained from LCP image divided by RCP image at the first incident angle of the x-ray (shown as yellow arrow in (a)). (c) PEEM image at the second incident angle of the x-ray, which is 180° away from the first angle respect to the sample normal (shown as green arrow in (a)). (d) PEEM image at the second incident angle of the x-ray, which is 90° away from the first angle respect to the sample normal (shown as purple arrow in (a)). (d) IP-PFM image of the area that imaged by PEEM.

Figure 6 XMCD of the selected pair of boxed areas in PEEM image. XAS curves are obtained with LCP incident x-ray. XMCD is calculated from the asymmetry of XAS curves between each pair of boxed areas.

Figure1

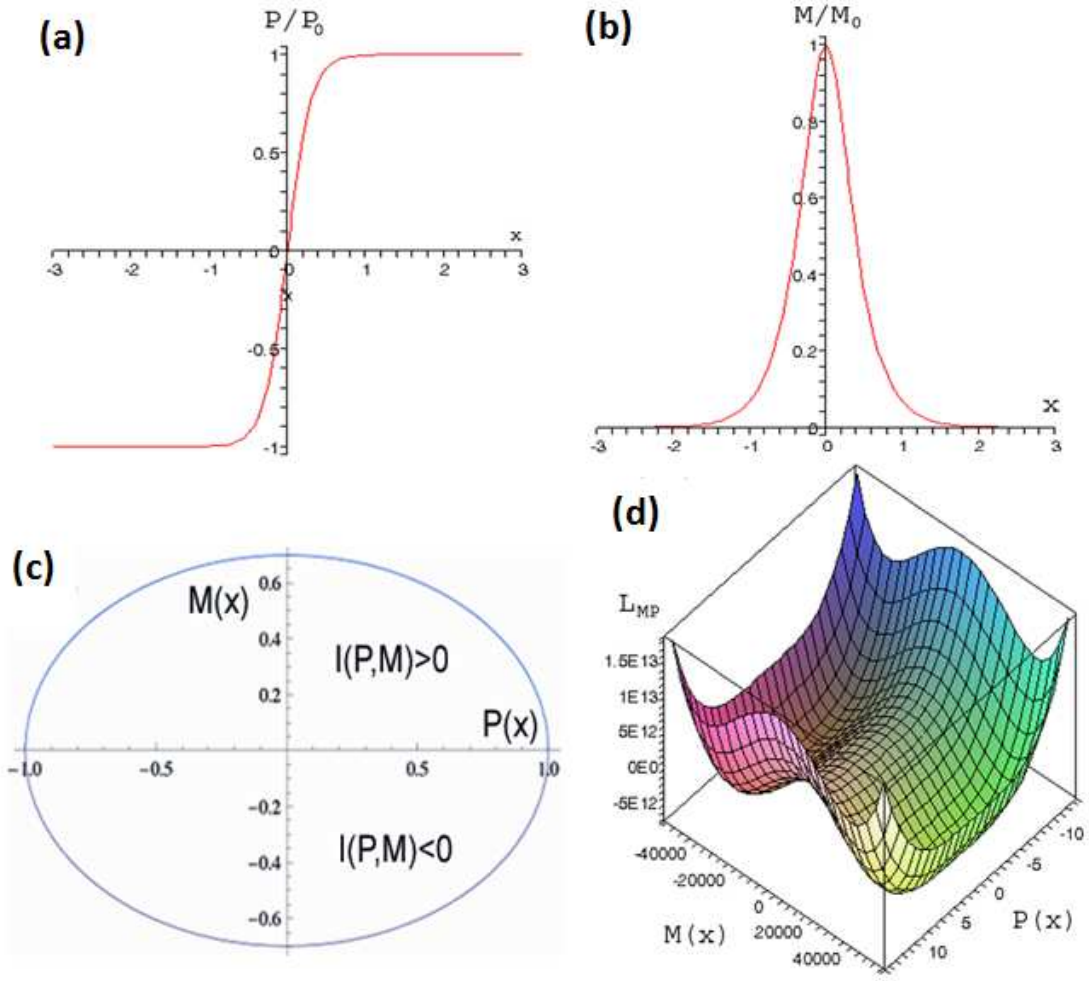

Figure 2

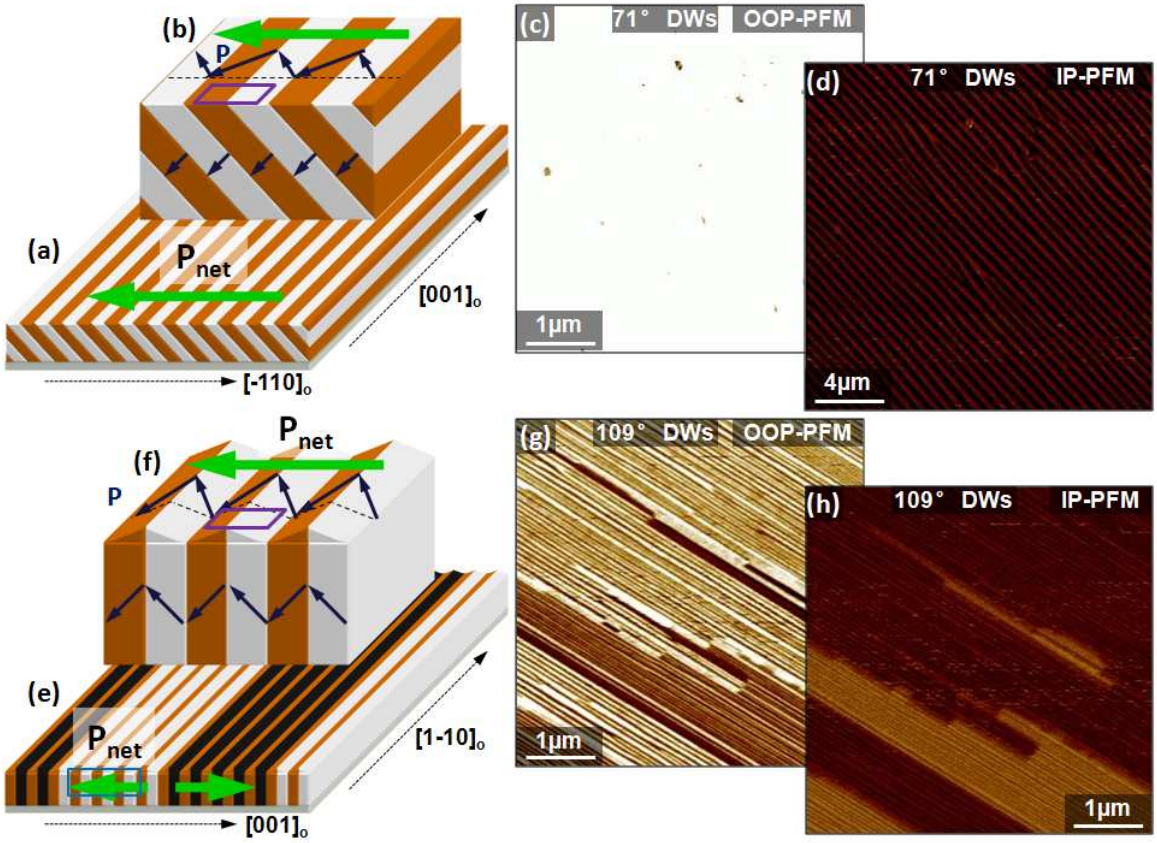
(b)
P
(a)
P net
[001]o
[-110]o
(c)
71° DWs
OOP-PFM
1μm
(d)
71° DWs
IP-PFM
4μm
P net
(f)
P
(e)
P net
[1-10]o
[001]o
(g)
109° DWs
OOP-PFM
1μm
(h)
109° DWs
IP-PFM
1μm

Figure 3

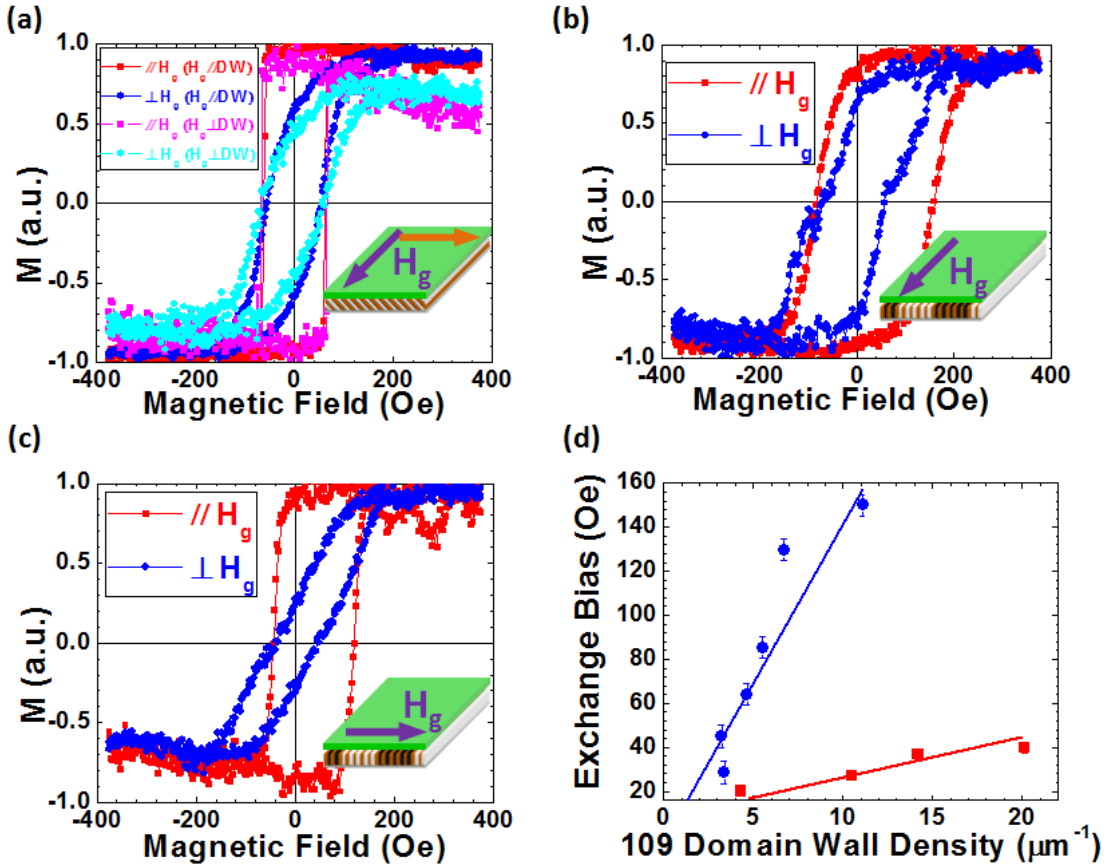
(a)
(b)
(c)
(d)
M (a.u.)
Magnetic Field (Oe)
// H_g
⊥ H_g
H_g
Exchange Bias (Oe)
109 Domain Wall Density (μm^-1)

Figure 4

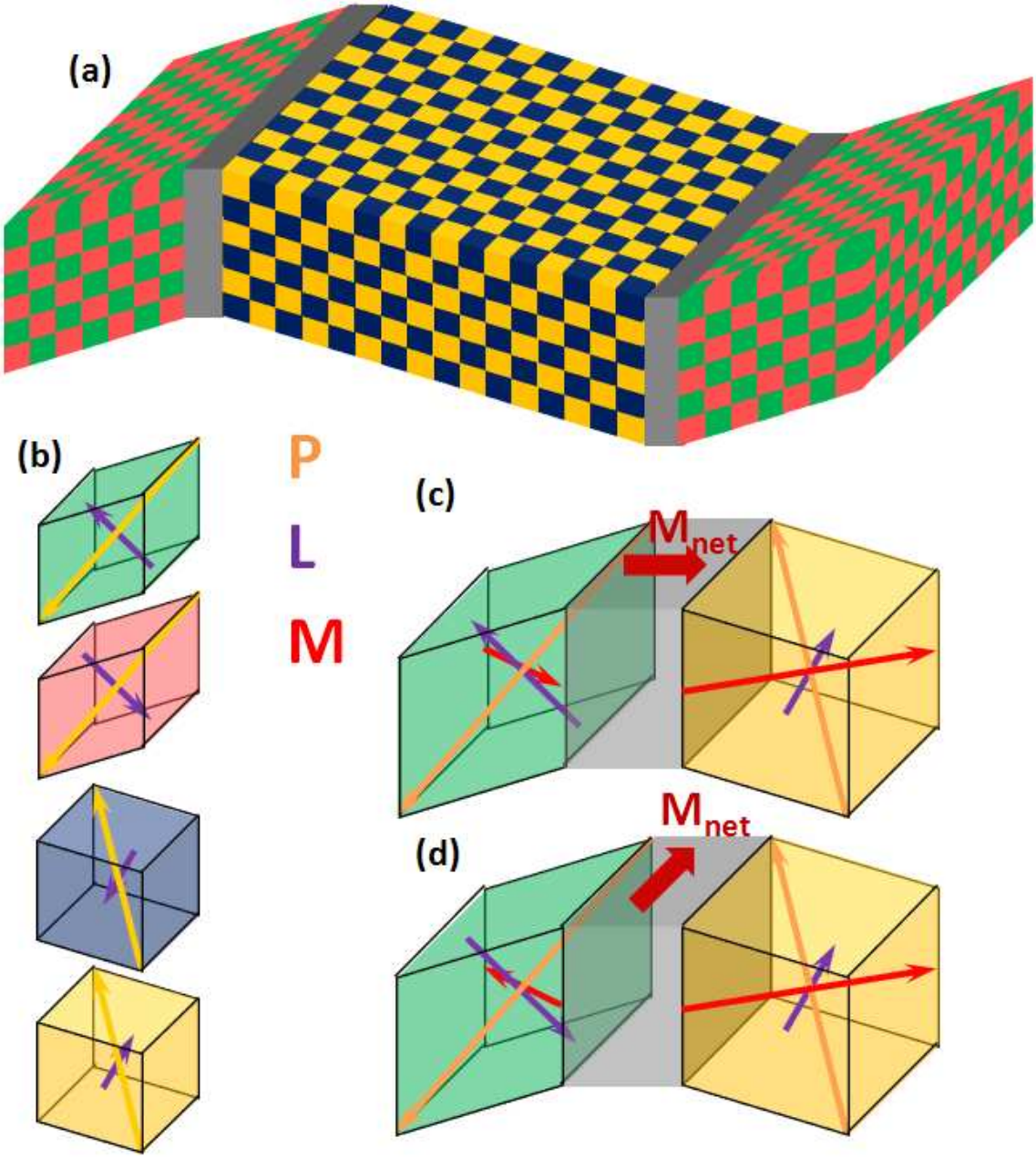

Figure 5

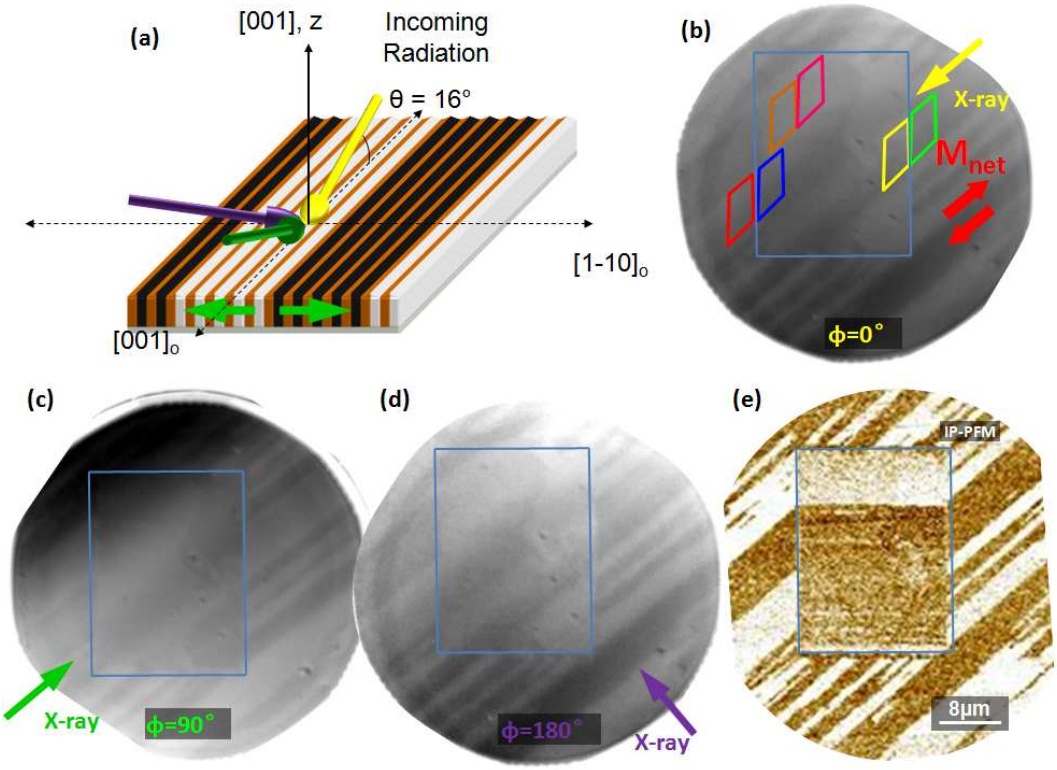
(a)
[001], z
Incoming
Radiation
θ = 16°
[1-10]o
[001]o
(b)
X-ray
Mnet
ϕ=0°
(c)
X-ray
ϕ=90°
(d)
ϕ=180°
X-ray
(e)
IP-PFM
8μm

Figure 6

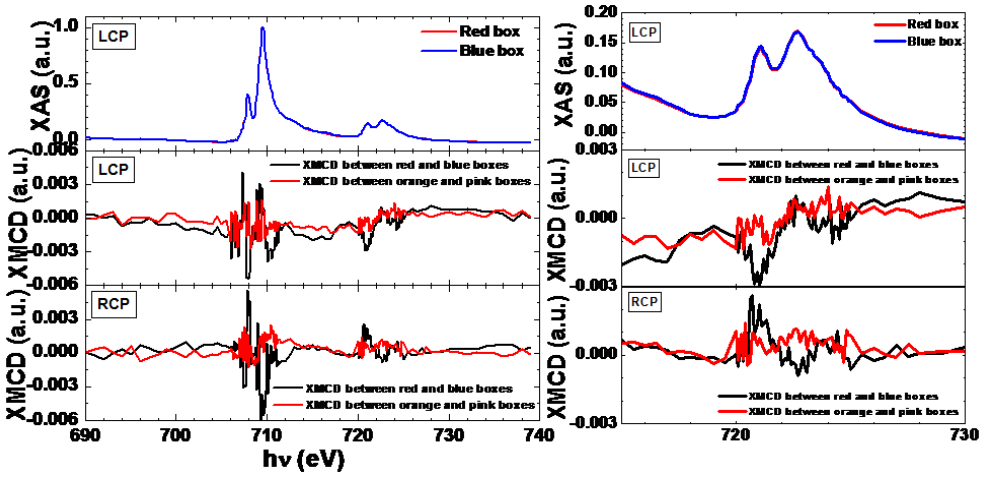

（三）心得及建議

計畫補助者特別感謝國科會與交通大學補助此次短期研究，這樣的補助有助於快速提升本校年輕教授快速累積研究能量，以利於其在交通大學建立其研究生涯。在出國期間有感國外名校如 UC Berkeley 之研究學者在學術的堅持與創新性，與其往來的兩個月內，有助於視野之開拓，更有助於加強語文與溝通能力。同時間可以了解目前國外研究之最新進展，提供新進人員在領域之選擇一個有用的參考資訊。綜合來說，雖然捨棄與家人團聚之機會，此次出國獲益甚多，希望以後能多多支持新進人員之補助申請案。